AIAA 94-0720
Unsteady Simulation of Flexible Missiles Flying Low Over The Sea

Daniel J. Lesieutre, Patrick H. Reisenthel,
Marnix F. E. Dillenius
Nielsen Engineering & Research, Inc.
Mountain View, CA

Danilo Viazzo, Steve Fisher, Sudarshan Bhat
Integrated Systems, Inc.
Santa Clara, CA

Samuel C. McIntosh
McIntosh Structural Dynamics
Mountain View, CA

32nd Aerospace Sciences Meeting & Exhibit
January 10-13, 1994 / Reno, NV

UNSTEADY SIMULATION OF FLEXIBLE MISSILES FLYING LOW OVER THE SEA

AIAA 94-0720

Daniel J. Lesieutre*, Patrick H. Reisenthel**, Marnix F. E. Dillenius†
Nielsen Engineering & Research, Inc.
Mountain View, CA

Danilo Viazzo‡, Steve Fisher***, Sudarshan Bhat++
Integrated System Inc.
Santa Clara, CA

Samuel C. McIntosh****
McIntosh Structural Dynamics
Mountain View, CA

ABSTRACT

A detailed investigation into the factors affecting transonic missile flight low over the sea has been performed. The simulation program developed in this effort models a flexible missile flying low over the sea and includes unsteady aerodynamics and detailed models of the control system, sensors, and structure. Unsteady aerodynamics are included in the simulation through the implementation of indicial theory. An extended six-degree-of-freedom model has been developed which includes control fin deflections and body elastic modes as additional system states. A sea wave/wind gust model has been developed which acts as an unsteady forcing function on the missile during its flight. The states of the system (6-DOF, fin deflections, and flexible body modes) are coupled and integrated together in the simulation. Unsteady aerodynamics can affect the performance of the missile directly or by excitation of the flexible body modes which can cause accelerations and spurious inputs at sensor locations.

NOMENCLATURE

a,b,c	complex curve fit coefficients
c.g.	center of gravity
C_P	pressure coefficient
$C_\varepsilon(t)$	indicial function
[D]	generalized damping matrix
GAF	generalized aerodynamic force
GF	generalized forcing vector
GIF	generalized indicial function
[K]	generalized stiffness matrix
[M]	generalized mass matrix
Q	system state vector
p,q,r	rotational rates
q_1-q_3	flexible body modes
t,τ	time
u,v,w	missile velocity
$\alpha,\gamma,\beta,\delta,\varepsilon$	curve fit coefficients
δ_1-δ_4	tail fin deflections
ϕ	aeroelastic mode shape

* Research Engineer, Senior Member AIAA
** Chief Scientist, Member AIAA
† President, Associate Fellow AIAA
‡ Research Scientist, Member AIAA
*** Section Manager, Flight Systems
++ Research Scientist
**** President, Associate Fellow AIAA

INTRODUCTION

Conventional flight simulation programs generally model the aerodynamics of a vehicle by pre-specifying the aerodynamic characteristics of the vehicle within a separate module. These characteristics are usually stored as either aerodynamic derivatives (for example, $C_{N\alpha}$) or as table look-up parameters as functions of flight conditions. This method of modeling the aerodynamics is fundamentally quasi-static and is usually augmented with aerodynamic damping derivatives such as C_{mq} to represent part of the unsteady effects. For flight low over the sea, as indicated in Figure 1, the flow environment is typically unsteady due to the presence of gusts from the waves and from atmospheric turbulence. Significant unsteady aerodynamic phase lags can occur under these adverse, often off-design, conditions which are not predicted by conventional methods. In addition, the strengths and frequencies of accelerations experienced by the missile due to the unsteady flow environment may excite structural bending modes of slender missiles. Therefore, to model sea skimming flight low over the sea, a method is required which models both the flexible missile and the unsteady aerodynamics.

A new simulation program has been developed which models a flexible missile flying low over the sea and includes effects of unsteady aerodynamics. The development of methods employed in the complete simulation program is described in References 1 through 3. The simulation contains detailed models of the missile guidance and control systems including the sensors and fin actuators. Unsteady aerodynamic responses of the vehicle are computed *off-line* and integrated into the overall simulation by employing indicial theory. Indicial theory allows unsteady aerodynamics to be modeled in an efficient manner. This paper describes the structure of the overall simulation program and the unsteady aerodynamic modeling of the vehicle. Simulation results are presented for flight over various sea states.

TECHNICAL APPROACH

This section describes the developed simulation program, the unsteady aerodynamic model, and verification tests used to validate the new approach. To predict the flight of a flexible vehicle, an augmented six-degree-of-freedom model is required which incorporates the flexible vehicle modes. The linearized airframe response of such a system is governed by the following differential equation:

$$[M]\{\ddot{Q}\}+[D]\{\dot{Q}\}+[K]\{Q\} = \{GAF\}+\{GF\}+\{\delta\} \quad (1)$$

where {Q} is a vector of the system states, [M], [D], and [K] are the generalized mass, damping, and stiffness matrices, respectively, {GAF} is the generalized aerodynamic force vector, {GF} is the generalized external forcing vector, and {δ} is the generalized control force vector.

The simulation program described herein models the dynamical system represented by Eqn. (1). The following section describes the simulation program in general terms. This is followed by a description of the vehicle structural model which provides the mass, damping, and stiffness matrices and the flexible vehicle modes. A description of the unsteady aerodynamic computational tool and a description of the calculation procedure used to obtain the generalized aerodynamic forces are then presented.

Simulation Structure and Design

To simulate the flight of a flexible missile flying in the unsteady flow regime low over the sea, it is necessary to accurately model the missile structure, the control system and sensors, the unsteady flow/gust environment, the unsteady aerodynamics, and their coupling. For this investigation, the modeled missile has the overall characteristics of the Harpoon[4] missile. However, many modeling assumptions have been made with respect to the control system and subsystem models which do not represent the actual missile.

Figure 2 depicts a block diagram of the overall simulation program. A detailed control system containing a radar altimeter model, an inertial measurement unit model (IMU), and an altitude control autopilot is included. In addition, a sea wave/wind gust model is implemented which acts as a forcing function to the coupled aero-servo-elastic system: aerodynamics - control system - flexible structure. Figure 3 shows details of the flexible 6-DOF kernel. To model the flexible missile and control fins, thirteen states are required: the standard six-degree-of-freedom states (u,v,w,p,q,r), the control fin deflection (δ_1-δ_4), and the first three body bending modes q_1-q_3 (pitch plane only). The state vector composed of these states is denoted as Q_j. The flexible 6-DOF kernel integrates the response of these thirteen coupled states subject to the unsteady sea wave gust forcing functions. The deterministic system states and the cross coupling of unsteady modes are depicted in Figure 4 in matrix form. Figure 4 shows the structure of the generalized aerodynamic force matrix and indicates the modes treated as unsteady modes in the current investigation. The pitch plane rigid modes w (plunge) and q (pitch), the control fin deflections δ_1-δ_4, and the body bending modes q_1-q_3 are treated as true unsteady modes, while others (u and the lateral modes) are treated in the conventional quasi-steady manner (i.e., using aerodynamic derivatives).

Descriptions of the radar altimeter, IMU, and fin actuator models follow.

Radar Altimeter Model

A radar altimeter is used to determine the altitude of the vehicle above the sea surface. Located in the nose of the missile, the radar model was designed to scan an area directly below it and up to 20 degrees ahead of the vehicle. This is modeled by extending four rays from the radar location, in the vehicle nose, toward the ground.

Given the frequency, phase, and amplitude of the wave (provided by the gust model described later), the wave deformations can be approximated as line segments connecting to each of the maximum amplitude points. This approximation is used to simplify the calculations required to determine the distances from each ray origin (radar source) and the first point where it intersects the wave. By measuring the distance from the radar to the approximate sea surface, and knowing the vehicle pitch orientation (given by the Inertial Measurement Unit - IMU) the altitude above the sea surface at each of the points may be determined. Each of the four ray altitudes are sorted and the minimum altitude is selected, since this would represent the largest signal return on a typical radar.

To reduce the frequency of changing altitudes as the missile is flying over various sea states the minimum altitude is processed. That is, the radar is measuring minimum altitudes at 800 Hz. At 200 Hz a processor samples the 800 Hz altitude and sorts this data to determine the minimum altitude. The processor then forwards the altitude to the control system at 200 Hz. To ensure the radar processor adapts to new sea state conditions during flight a reset switch is activated at 10 Hz. This reset switch clears the minimum altitude in the processor memory and replaces it with the latest measurement.

Inertial Measurement Unit (IMU) Model

The inertial measurement unit (IMU) is used to measure rotational rates and vehicle orientations for the control system. The IMU design contains a gyroscope and an accelerometer. The inputs of the IMU model are true body rates and true body accelerations generated in the Generalized Aerodynamic Force Kernel block. The outputs of the IMU are pitch rate and an estimated Euler pitch angle. To reduce the complexity of the model, the IMU model was derived based upon a flat and non-rotating earth. This assumption allows for the inertial frame to be coincident with the North-East-Down (NED) reference frame.

The gyroscope model includes error sources based upon one-sigma values listed in Table 1. These errors reflect typical values that may be found in an IMU. The inputs to the gyro are the body rates and the accelerations in the body frame. The measured body rates formed from the true inputs and error sources are summed and output as the measured rates. These rates are then processed to form body orientations. The process calculation is based upon using quaternions to form the directional cosine matrix and then extracting the vehicle orientation from specific elements in the directional cosine matrix.

TABLE 1 Gyro Errors

Parameter	Metric Value
Bias	4.85e-6 (rad/s)
Scale Factor	5.00e-4
Off Axis Scale Factor	3.30e-4
Asymmetric Scale Factor	6.70e-5
Thermal Bias Shift	4.85e-8 (rad/s)
Mass Unbalance	1.60e-6 (rad/s/m/s^2)
Quadrature	8.24e-7 (rad/s/m/s^2)
G^2 Sensitivity	3.36e-9 (rad/s/m2/s^4)

The accelerometer is modeled in much the same way as the gyro. Since the accelerometer is offset from the center of gravity, the IMU will measure additional accelerations from vehicle rotation rates. As with the gyro model the error sources are added together. Table 2 lists the one-sigma error used from the accelerometer model.

TABLE 2 Accelerometer Errors

Parameter	Metric Value
Scale Factor	5.00e-4
Off Axis Scale Factor	1.00e-5
Asymmetric Scale Factor	-1.24e-5 x-axis
	9.58e-5 y-axis
	-5.91e-5 z-axis
G^2 Sensitivity	3.36e-9 (rad/s/m^2/s^4)

Actuator Model

The Harpoon missile modeled in this simulation utilizes four aerodynamic fins for controlling the vehicle. Due to the lack of available data for Harpoon actuator models, a simple second order actuator was adopted. The block diagram of this model is shown in Figure 5. The transfer function of this model can be written as

$$\frac{\delta_{Actual}}{\delta_{Command}} = \frac{\omega^2}{s^2 + 2\zeta\omega s + \omega^2} \qquad (2)$$

where δ_{Actual} and $\delta_{Command}$ are the actual fin deflection and commanded position of the fin deflection from the control system, respectively. A natural frequency, ω, of 125 rad/sec and a damping ratio, ζ, of 0.7 was chosen to give the model approximate responsive linear characteristics of a typical missile actuator. This model does not capture any of the nonlinear characteristics of actuators such as rate limits, dead bands, or hysteresis. Since this simulation's focus is not to utilize high fidelity models, neglecting the nonlinear characteristics does not detract from using the indicial functions for aerodynamic models.

Structural Modeling

A finite element beam model of the missile has been developed to provide the first three structural body bending modes. These modes are shown in Figure 5 and are used as additional system states in the simulation.

A structural model for the body was derived from NASTRAN data for the Harpoon Block 1D, air launch configuration. The model was constructed from beam bending elements, with a total of 61 nodes and 120 degrees of freedom. Beam properties were taken directly from the NASTRAN data. Concentrated masses to account for equipment and fuel were also included. Frequencies and mode shapes were calculated for both full fuel and partial (50%) fuel. The codes SAMGEN (for the finite-element model) and VIBE (for the modal analysis) were used (Ref. 5).

VIBE and NASTRAN frequencies for the first three elastic modes are compared in Table 3. The higher VIBE frequencies are attributable to the lack of transverse shear effects in the SAMGEN beam model. The mode shapes from VIBE are shown in Figure 6; these compare very well with the NASTRAN mode shapes. The frequency differences are not considered to be significant, since all that is needed is a reasonable representation of a flexible missile body.

TABLE 3. Strucutral Frequency Comparisons (full fuel)

Body Mode	NASTRAN	SAMGEN/VIBE
1	45.83	48.09
2	109.0	127.2
3	171.8	211.8

In addition to the added states in the simulation, elastic motion of the body also provides inputs to the radar altimeter and the IMU. Displacements and bending rotations at the radar altimeter and IMU locations were therefore supplied for each mode.

Unsteady Aerodynamic Approach

The development of an overall flight simulation program applicable to analysis and design which includes unsteady aerodynamics, structural elastic behavior, and the detailed modeling of a control system requires a computationally efficient means of representing accurate unsteady aerodynamics and unsteady forcing due to sea waves. The unsteady aerodynamics of the missile are obtained with indicial theory. Previous papers, Refs. 2 and 3, have demonstrated that indicial theory is valid for sea skimming cruise conditions. Program TSDVRT,[2,3] based on CAP-TSD,[6] has been developed to compute time accurate unsteady solutions to the flow over missile configurations based on transonic small disturbance flow approximations. The program also allows accounting for the effects of streamwise vorticity. Program TSDVRT is employed to compute the generalized indicial functions (GIF) for each of the system states (Q_j) shown in Figure 4. These indicial responses are aerodynamic responses of the missile to step changes of each of the unsteady system states (indicated in Figure 4) and are used to generate the associated generalized aerodynamic forces acting on the missile. These indicial responses are included in the overall simulation using Duhamel's convolution theorem

to obtain the response to an arbitrary forcing function associated with the system modes in the pitch plane (either rigid, flexible, or due to gusts). A brief description of the rationale for using indicial functions and their range of application is given below, followed by a description of the calculation procedure used to obtain the GAFs and GIFs.

Rationale Behind the Use of Indicial Functions

In this investigation, the unsteady aerodynamic characteristics are determined from the *indicial functions* of the body and fin loads, i.e., the responses to step inputs in various structural modes, including flexible and rigid body modes. A significant advantage of this approach, when it is applicable, is that the aerodynamic response to complex unsteady stimuli such as deformations associated with multiple aeroelastic modes may be predicted solely from the knowledge of the indicial functions. These functions, require only one calculation per modal deformation about a given mean configuration (trimmed cruise condition, for example). The multiple flexible modes may occur in a wide range of frequencies which may be excited as a consequence of rapid maneuver, gusts due to the presence of the sea waves, or by control inputs to various actuators of the control fins. Therefore, the indicial theory approach represents a considerable reduction in unsteady aerodynamics computational requirements, especially in view of the large number of parameters involved in any simulation. Reference 3 shows that indicial theory may be applied to sea skimming missile flight by demonstrating the accuracy of the method when compared with direct numerical simulations. Since the current work relies on the use of the indicial functions, an overview of indicial theory and the conditions under which the indicial method is expected to apply are presented.

If it can be assumed that the change in a given system response, denoted as C(t), is linear with respect to a boundary condition (or forcing function) ε, then the time response of the system to an arbitrary forcing of the parameter ε may be represented by Duhamel's convolution integral theorem:

$$C(t) = C_\varepsilon(t)\varepsilon(0) + \int_0^t C_\varepsilon(t-\tau)\,\frac{d\varepsilon(\tau)}{d\tau}\,d\tau \qquad (2)$$

where $C_\varepsilon(t)$ is the *indicial function* corresponding to a step change in ε. The implication of the Duhamel convolution integral is that, under the linearity assumptions C(t) can be analytically predicted for any arbitrary change in the forcing parameter ε, provided that the *indicial response*, $C_\varepsilon(t)$, is known. The power of Equation 2 resides in the fact that the response C(t) may be calculated from the knowledge of the excitation parameter ε and the indicial response C_ε, which requires only a single experimental or numerical determination.

Therefore, for the indicial method to be applicable to the present problem, the generalized aerodynamic forces must behave linearly with respect to the amplitude of a given aeroelastic or rigid-body mode under consideration. The indicial function, $C_\varepsilon(t)$, must also be independent of the time instant at which the step in ε is applied. Although the range of validity of the first of these requirements may be directly evaluated by recording unsteady load variations for various amplitudes of the step-input disturbance, the latter requirement constitutes a somewhat less tangible condition which must be verified by different means. To this end, one uses the convolution integral, Eqn. (2), to predict the linear phase and amplitude response of the oscillatory load C(t), in response to a harmonic perturbation of the type: $\varepsilon = e^{ikt}$. At large times, the response predicted using Eq. (2) must also be time periodic, therefore: $C(t) = Ae^{i\Delta\phi} \times e^{ikt}$, where the amplitude A(k) and phase change $\Delta\phi(k)$ are *predicted* by integrating Eqn. (2) using $\varepsilon(t) = e^{ikt}$. If the results of direct numerical calculation of C(t) in response to oscillatory modal excitations exhibit phase and amplitude characteristics which are close to those predicted by application of Duhamel's convolution integral, then it may be concluded *a posteriori* that the linearity conditions which constitute the theoretical foundation of the indicial theory are satisfied.

Figure 7 depicts a typical indicial response for the pitching-moment coefficient ΔC_m, as a result of body elastic mode deformation. The Duhamel convolution integral is used to predict the unsteady aerodynamic amplitude and phase lags of the response to harmonic excitation of this mode shape. Figure 8 compares results from the convolution of the indicial response with results from direct numerical simulations using program TSDVRT. This comparison indicates that indicial theory is valid for these conditions. Additional verifications of the approach are contained in Reference 3.

GAF and GIF Calculations Using Indicial Theory

This section defines the generalized aerodynamic forces (GAF) required by the simulation in terms of the generalized indicial functions (GIF) calculated by program TSDVRT.[3] This is followed by a description of the method used to include the GIFs into the simulation to calculate the GAFs during the vehicle flight trajectory. At any point in the simulation, the generalized aerodynamic force vector $\{GAF_i(t)\}$ is given by:

$$\{GAF_i(t)\} = \sum_j [GAF_{ij}(t)] \qquad (3)$$

where $[GAF_{ij}(t)]$ is the GAF matrix whose individual terms GAF_{ij} correspond to the effect of deformation of mode i on mode j. The sum in Eqn. (3) is carried out over all the modeled modes, rigid, flexible, and control. For this investigation, only pitch plane states are considered, w, q, δ_1-δ_4, and q_1-q_3. Each term in the GAF_{ij} matrix consists of a dual generalized indicial function included in the Duhamel convolution integral:

$$GAF_{ij}(t) = GIF1_{ij}(t)Q_j(0) + \int_0^t GIF1_{ij}(t-\tau)\dot{Q}_j(\tau)\,d\tau \qquad (4)$$

$$+ GIF2_{ij}(t)\dot{Q}_j(0) + \int_0^t GIF2_{ij}(t-\tau)\ddot{Q}_j(\tau)\,d\tau$$

The dual indicial function formulation arises from the nature of the boundary conditions employed in the unsteady aerodynamic program TSDVRT.[3] The first indicial function corresponds to a pure deformation boundary condition of mode Q_j, while the second indicial function corresponds to its derivative or *apparent mass* boundary condition (see Ref. 3).

For either the deformation or the apparent mass boundary conditions, the generalized indicial functions are obtained by running the TSDVRT[3] program for step changes in each of the boundary conditions of each of the unsteady system states Q_j. The mode shape corresponding to state Q_j is defined as ϕ_j. The generalized indicial function matrix $GIF_{ij}(t)$ is defined as the integral over the entire vehicle surface of the pressure distribution corresponding to deformation of mode ϕ_i projected onto the mode shape ϕ_j:

$$GIF_{ij}(t) = \iint_S -C_{P_{\phi_i}}(x,y,z;t)\vec{\phi}_j(x,y,z)\, ds(x,y,z) \quad (5)$$

Therefore, to calculate the complete GIF matrix, program TSDVRT need only be run once for each mode shape ϕ_i (actually twice, once for the deformation boundary condition and once for the apparent mass boundary condition). Equation 5 is programmed within TSDVRT and provides a whole (time-dependent) column of the GIF_{ij} matrix for each computer run. For the 9 unsteady modes modeled in this investigation, there are $9^2 \cdot 2 = 162$ GIF_{ij}s which need to be calculated in advance for the simulation program.

The simulation program requires the GAFs given by Eqn. (4) to be determined at each time step. The GIFs which are predetermined by program TSDVRT are recorded as discrete-times functions [t(k),GIF_{ij}(k)]. With this discrete representation, numerical evaluations of the integrals in Eqn. (4) are required. Numerical convolution of all 162 indicial functions at every time step in the simulation was determined not to be computationally practical. To make the indicial function formulation efficient for the simulation program, the discrete-time indicial functions are curve fit with a series of expontential/trigonometric functions. The benefit of this functional representation of the indicial functions is twofold: 1) the indicial functions' determination and their curve fitting are performed once outside of the simulation, and 2) the chosen functional form of the curve fit allows the Duhamel convolution integral for the GAFs to be replaced with simple ordinary differential equations that can be integrated in time simultaneously with the standard 6-DOF and elastic states. The functional form of the curve fit is given by:

$$GIF(t) = \alpha + \sum_{n=1}^{N} \gamma_n e^{-\beta_n t}\cos(\delta_n t + \varepsilon_n) \quad (6)$$

This functional representation is very robust and allows complex indicial functions to be accurately represented, including indicial functions with harmonic unsteady responses as $t \to \infty$. A numerical optimization method[7] is employed to determine the curve fit coefficients. Details of this procedure are contained in Reference 8. For this investigation, retaining 6 terms (N) in the series of Eqn. (6) has proved sufficient to fit very complex indicial functions. Figure 9 demonstrates the ability of this curve fitting procedure.

The curve fit of the indicial function given by Eqn. (6) can also be expressed for convenience with exponentials of complex variables. This notation for GIF1 and GIF2 given in Eqn. (4) is expressed as:

$$GIF1_{ij}(t) = Re\{a_{ij} + \sum_n c_{ijn} e^{-b_{ijn}t}\}$$

$$= Re\{a_{ij} + \sum_n \xi_{ijn}(t)\} \quad (7)$$

$$GIF2_{ij}(t) = Re\{a'_{ij} + \sum_n c'_{ijn} e^{-b'_{ijn}t}\}$$

$$= Re\{a'_{ij} + \sum_n \xi'_{ijn}(t)\} \quad (8)$$

The coefficients in Equation (10) are complex and related to those of Eqn. (6) as follows:

$$a_{ij} = \alpha_{ij} \qquad b_{ij} = \beta_{ij} + i\delta_{ij} \qquad c_{ij} = \gamma_{ij}(\cos\varepsilon_{ij} + i\sin\varepsilon_{ij}) \quad (9)$$

where $i^2 = -1$.

Using the complex representations of the GIF_{ij} given by Eqn. (7) in the GAF_{ij} given by Eqn. (4) yields:

$$GAF1_{ij}(t) = Re\{\sum_n \xi_{ijn}(t)Q_j(0) + a_{ij}Q_j(t) + \sum_n \psi_{ijn}(t)\} \quad (10)$$

where ψ_{ijn} is given by:

$$\psi_{ijn}(t) = c_{ijn}\int_0^t GIF1_{ij}(t-\tau)\dot{Q}_j(\tau)\,d\tau \quad (11)$$

As previously mentioned, this calculation is replaced in practice by a simple differential equation:

$$\dot{\psi}_{ijn}(t) = -b_{ijn}\psi_{ijn}(t) + c_{ijn}\dot{Q}_j(t), \quad \psi_{ijn}(0) = 0 \quad (12)$$

Similar expressions exist for GAF2 where the coefficient a,b,c are replaced with a',b',c', and Q_j is replaced with $\dot{Q}_j$.

Sea Wave and Gust Model

This section describes the ideal sinusoidal sea wave and gust model employed in the simulation. The height of the sea surface below the missile is defined as:

$$h_{wave} = h_w \sin[(2\pi/\lambda_w)(U_w t + U_m t + x_o + x)] \quad (13)$$

where h_w = amplitude given by the maximum wave height, λ_w = wave length, U_w = wave propagation speed, U_m = missile speed, x_o = initial missile c.g. location, and x = initial x offset

The vertical gust velocity, due to the wave plunging motion as a function of altitude h, is obtained from solution of the wave equation and is given by:

$$v_{g1} = h_w \cos[f(U_w t + U_m t + x_o + x)] f U_w e^{-fh} \qquad (14)$$

where $f = 2\pi/\lambda_w$, and h = altitude of the missile. The exponential factor in the above expression is the attenuation of the gust amplitude with increasing altitude. In addition to the wave plunging motion, there is an additional gust component due to the wind blowing over a wavy surface. This gust component also obtained from solution of the wave equation is given by:

$$v_{g2} = h_w \cos[f(U_w t + U_m t + x_o + x)] f(U_w - U_{wind}) e^{-fh} \qquad (15)$$

where, U_{wind} designates the wind speed. The effect of any atmospheric turbulence near the sea surface was not accounted for in this investigation.

In the simulation program, the total vertical gust $v_g = v_{g1} + v_{g2}$ is used as an unsteady forcing function. The generalized aerodynamic forcing vector due to gusts $\{GF_i(t)\}$ (Eqn. 1) is obtained in a manner similar to the generalized aerodynamic force vector described in the previous section. Program TSDVRT is used to obtain the generalized indicial function responses of the vehicle to a *step change in the gust mode*. This step change in the gust mode is defined by the vehicle flying into a semi-infinite sharp-edged gust. Generalized indicial responses to a semi-infinite sharp-edged gust are calculated for each of the system states and implemented in the simulation as the forcing functions in the dynamical system as modeled by Eqn. 1.

SIMULATION RESULTS

Simulations have been performed for a flexible missile flying low over the sea. Results are presented for Mach numbers of 0.8 and 2.0 and for sea states 3, 5, and 7. When the simulation is initially started the radar altimeter is not equilibrated. For this reason, the simulation is run for ten seconds before the missile is commanded to fly low over the sea. The first ten seconds are used to eliminate transients due to assumed initial conditions.

M_∞ = 0.8, Sea State 3

Figure 10 illustrates a typical trajectory of a flexible missile (3 bending modes, 48, 127, and 212Hz) flying low over the sea at M_∞ = 0.8 and sea state 3. The missile is assumed to be flying in a direction perpendicular to the wave fronts. The variations in altitude, vertical acceleration, pitch angle, control fin deflection angle, and the amplitude of the 1st body bending mode are shown in Figure 10. The waves are shown in the upper graph of this figure. The missile flies free for the first 10 seconds and then is commanded to fly at 3 meters above the mean sea. This maneuver at t = 10 is evident in the results. The mean *steady state* pitch angle of 6.6 degrees is approximately the trim angle of attack. The mean *steady state* trim deflection angles are approximately -1.8 deg. (leading edge down) with maximum unsteady variations of 0.1 degs. Note that the tail fins are in the X orientation. The maximum unsteady vertical acceleration experienced by the missile is $1.4 m/s^2$. The modal deformation of the 1st body bending modes is also shown in the figure (variable phi 1).

M_∞ = 0.8, Sea State 5

Results for sea state 5 are shown in Figure 11. The sea state 5 results differ from sea state 3 in two respects: the wave length is longer (170m versus 71m) and the gust velocities are higher (2m/s versus <0.5m/s). The longer wave length does not significantly affect the behavior of the missile. The stronger gust velocities result in larger unsteady aerodynamic forces and moments, and higher unsteady accelerations and pitch rates. However, these conditions do not adversely affect the missile's ability to fly low over the sea.

It should be noted that the sea skimming missile modeled is large and heavy requiring a trim angle of 6.6 deg. or 31m/s downwash to fly at trim, where lift equals weight. Unsteady forcing of 2m/s is only a small fraction of the trim downwash. A lighter, more dynamic, and/or more flexible missile with a smaller trim angle of attack may have a significantly different unsteady behavior which may adversely affect control of the missile.

M_∞ = 0.8, Sea State 7

Results for sea state 7 are shown in Figure 12. The wave length for sea state 7 is 455m and the gust velocities are 7m/s. The extremely long wave length causes the missile to try to follow the troughs in the waves. The stronger gust velocities result in larger unsteady aerodynamic forces and moments, and higher unsteady accelerations. However, these conditions do not adversely affect the missile's ability to fly low over the sea.

M_∞ = 2.0

The flight trajectories corresponding to sea states 3, 5, and 7 for M_∞ = 2.0 are shown in Figure 13, and the vertical accelerations are depicted in Figure 14. The mean *steady state* pitch angle for this flight condition is 1.1 degs., and the mean tail fin deflection angles are approximately -0.4 deg. For sea state 3, the missile experiences unsteady accelerations of approximately $\pm 5 m/s^2$ about the 1-g mean. The stronger wave/wind induced gust velocities at sea state 5 result in larger unsteady aerodynamic forces and moments, and higher unsteady accelerations ($\pm 8 m/s^2$). The even stronger gust velocities for sea state 7 result in even larger unsteady aerodynamic forces. The weight of the missile is 5000N and it experiences unsteady loads of approximately ±4000N.

Note that for a flight speed corresponding to M_∞ = 2.0 at sea level, the missile experiences both positive and negative gusts at a frequency such that by the time the missile can react to a positive gust, it experiences a negative gust. As a consequence, the missile can maintain

flight low over the sea even though it is experiencing large unsteady forces. While the magnitude of the unsteady forces is large, it does not affect the ability of the control system and autopilot to maintain flight low over the sea for the case under consideration.

Rigid and Flexible Missile for Sea State 5

A comparison of rigid and flexible missile simulations for sea state 5 at $M_\infty = 0.8$ yields nearly identical results. To obtain the rigid body results, the flexible modes within the simulation were turned off ($Q_{11} = Q_{12} = Q_{13} = 0$). Figure 15 depicts the actual difference by subtraction of the flexible results from the rigid results on a magnified scale. For the missile modeled, the flexible modes have virtually no effect on the overall 6-DOF system states. This is due primarily to the large mass and moment of inertia characteristics of the modeled missile, and the lack of a strong coupling between the aeroelastic modes and the control system components.

CONCLUSIONS

A new comprehensive simulation method has been developed which models a flexible missile flying low over the sea. The method includes effects of unsteady aerodynamics, flexible or rigid missile structure, and flight control systems and sensors. The simulation is unique in that unsteady aerodynamic effects are modeled using a computationally efficient method based on the use of indicial functions, thereby allowing a practical representation of full aero-servo-elastic coupling effects in the overall simulation.

For the configuration investigated, a Harpoon type missile, the control system is able to maintain safe flight low over the sea. The missile modeled is large and heavy with large moments of inertia requiring a trim angle of 6.6 deg. (or 31m/s downwash) to fly at a condition where lift equals weight for $M_\infty = 0.8$. The unsteady gusts from the sea are only a small fraction of the trim downwash which does not significantly affect the flight of the missile. Significant unsteady loads are experienced by the missile (±750N for a missile weight of 5000N) for the higher sea states, but because the missile inertia characteristics are high, the effects of these unsteady loads do not adversely affect its flight. A lighter, more dynamic missile having a smaller trim angle of attack may have a significantly different unsteady behavior. The effects of the flexible vehicle modes are found not to adversely affect the flight of the present vehicle compared to a rigid missile. For a flexible missile with bending modes of lower frequency (closer to the gust forcing frequency), adverse effects may arise due to coupling. The comprehensive simulation methodology described here is a tool which allows the evaluation of such effects.

The $M_\infty = 2.0$ results indicate that the missile control system can maintain flight at supersonic Mach numbers. The missile trim angle of attack is lower because the missile speed and hence dynamic pressure is higher than for the $M_\infty = 0.8$ cases. For sea state 7 the missile experiences unsteady loads of approximately ±4000N. While the magnitude of the unsteady forces (forcing function) is large, it does not affect the ability of the control system and autopilot to maintain flight low over the sea. This is due to the very fast flight speed and inertial characteristics of the missile, as it does not "have time" to react to an upward gust before it experiences a downward gust. Again, a lighter, more dynamic missile is expected to experience larger unsteady aerodynamic effects.

The most limiting factor in the present accuracy of the overall simulation is the model of the sea as a single frequency sine wave. To be more accurate, the sea (i.e., its surface and, in particular, the turbulent environment at high sea states) must be modeled using a broadband multiple frequency representation. The latter can be based on available data.

ACKNOWLEDGMENTS

The authors wish to acknowledge the role of Naval Surface Warfare Center, White Oak Laboratory, in sponsoring this research effort under a Phase II SBIR Contract N60921-90-C-0134 with Mr. Gil Graff as technical monitor.

REFERENCES

8. Lesieutre, D. J., Reisenthel, P. H., Dillenius, M. F. E., Vaizzo, D., Fischer, S., Sudarshan, B., and McIntosh, S. C.: Unsteady Simulation of Flexible Missiles Flying Low Over The Sea, NEAR TR 465, October 1993.
2. Reisenthel, P. H. and Nixon, D.: Prediction of Unsteady Separated Transonic Flow Around Missile Configurations, AIAA Paper 91-0601, January 1991.
3. Reisenthel, P. H., Lesieutre, D. J., and Nixon, D.: Prediction of Aeroelastic Effects For Sea-Skimming Missiles With Flow Separation, AIAA Paper 91-1052, April 1991.
4. Harpoon Weapon System Development Phase Stability and Control Report, MDC E1152, October, 1974.
5. McIntosh, S. C., Jr.: Optimization and Tailoring of Lifting Surfaces with Displacement, Frequency, and Flutter Performance Requirements. NWC TP 6648, April 1987, Naval Air Warfare Center Weapons Div., China Lake, CA.
6. Batina, J. T., Seidel, D. A., Bennett, R. M., and Bland, S. R.: Preliminary Users Manual For CAP-TSD, NASA Langley, December 1987.
7. Powell, M. J. D.: An Efficient Method for Finding the Minimum of a Function of Several Variables without Calculating Derivative, Computation Journal, Volume 7, 1964, pp. 155-162.
8. Lesieutre, D. J.: Software Design Document for CSCI Program EXPFIT, NEAR TR 467, Volume 2, May 1993.

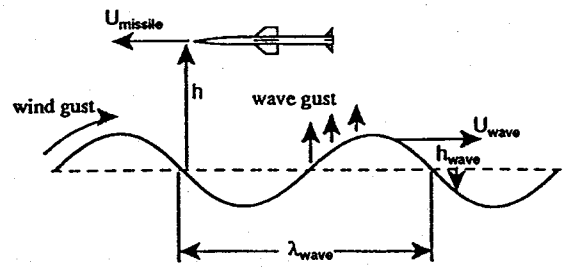

Figure 1.- Typical sea skimming missile geometry and flight profile.

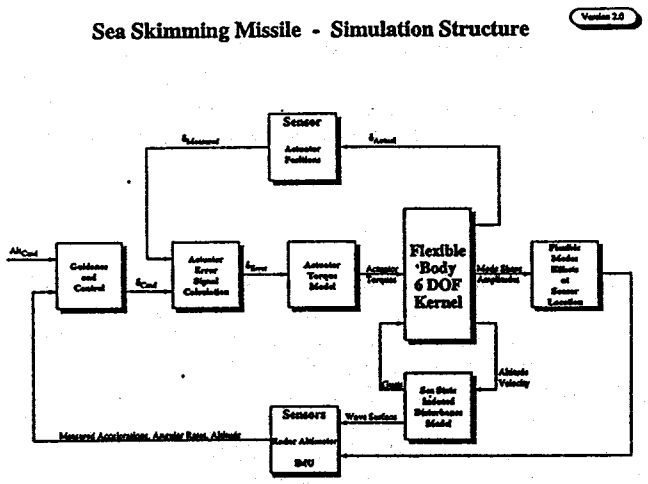

Figure 2.- Block diagram of the overall simulation program.

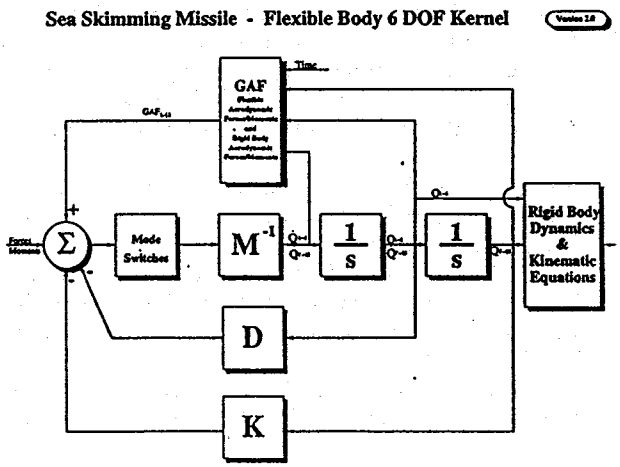

Figure 3.- Block diagram of the flexible 6-DOF kernel.

Missile States

mode #	mode	u	v	w	p	q	r	δ_1	δ_2	δ_3	δ_4	q_1	q_2	q_3
1	u													
2	v													
3	w			*		*		*	*	*	*	*	*	*
4	p													
5	q			*		*		*	*	*	*	*	*	*
6	r													
7	δ_1			*		*		*	*	*	*	*	*	*
8	δ_2			*		*		*	*	*	*	*	*	*
9	δ_3			*		*		*	*	*	*	*	*	*
10	δ_4			*		*		*	*	*	*	*	*	*
11	q_1			*		*		*	*	*	*	*	*	*
12	q_2			*		*		*	*	*	*	*	*	*
13	q_3			*		*		*	*	*	*	*	*	*
14	v_g			*		*		*	*	*	*	*	*	*

* indicates unsteady mode

Figure 4.- Simulation state variable matrix.

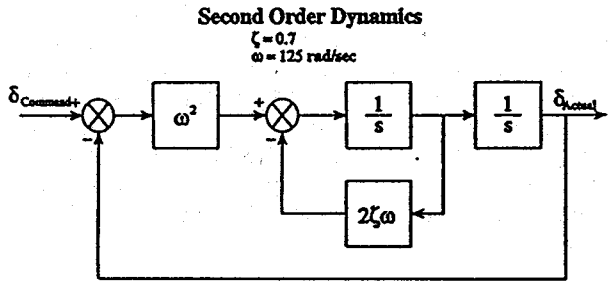

Figure 5.- Actuator model block diagram.

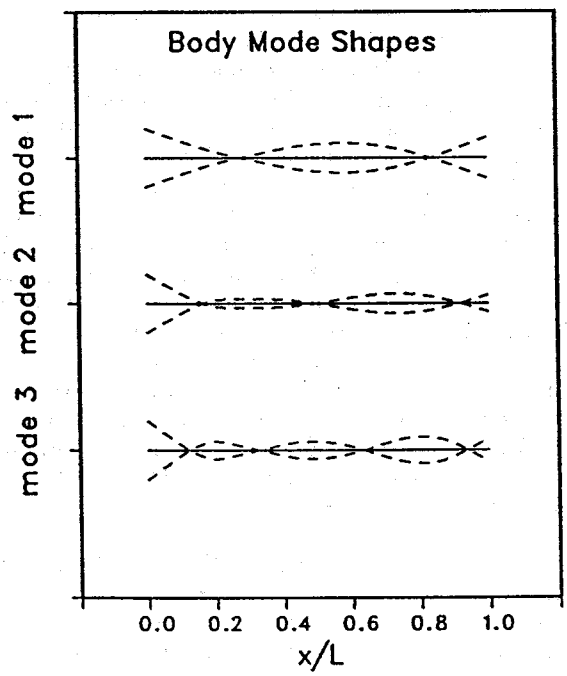

Figure 6.- Predicted first three missile body bending modes.

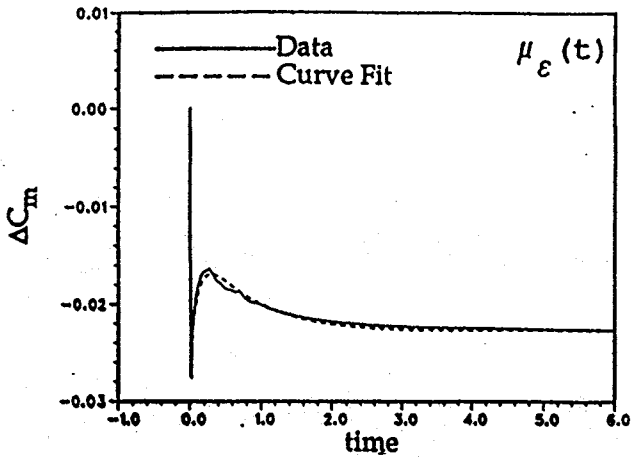

Figure 7.- Pedicted and curve fit pitching moment indicialfunction due to deformation of a body bending mode.

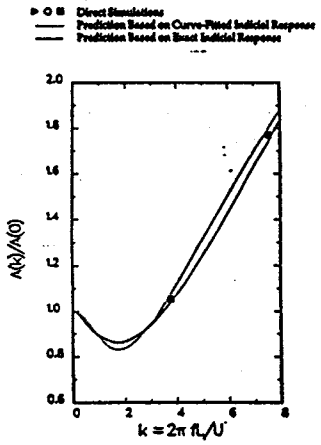

Figure 8.- Comparison of amplitudes and between indicial-theoretical prediction and direct numerical simulations for C_m.

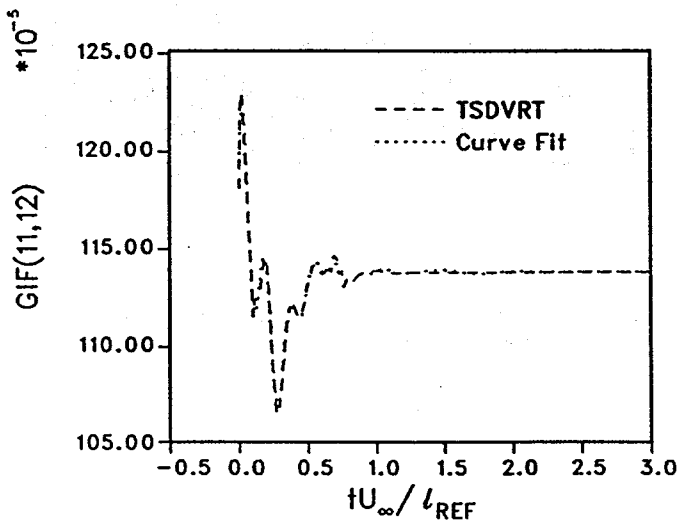

Figure 9.- Calculated and curve fit generalized indicial function due to 1st body bending mode (11) on 2nd body bending mode (12).

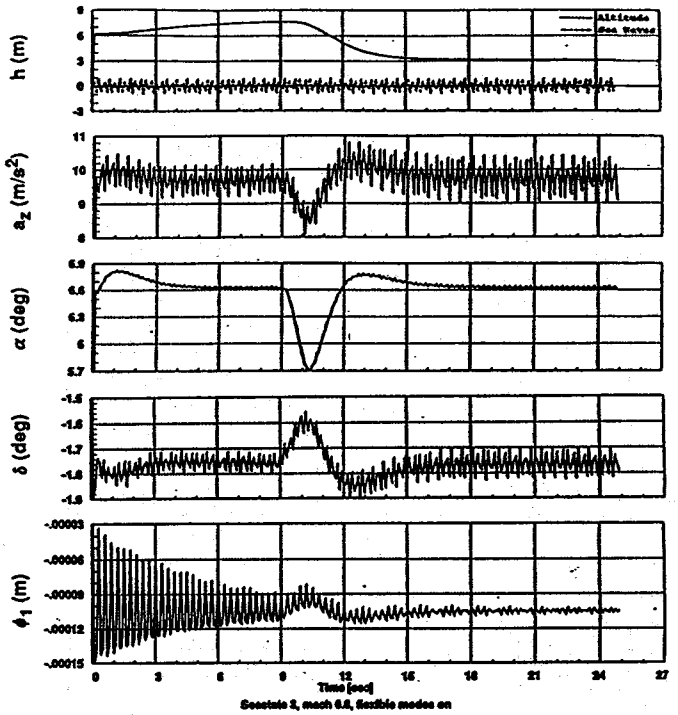

Figure 10.- Flexible simulation results for $M_\infty = 0.8$ and sea state 3.

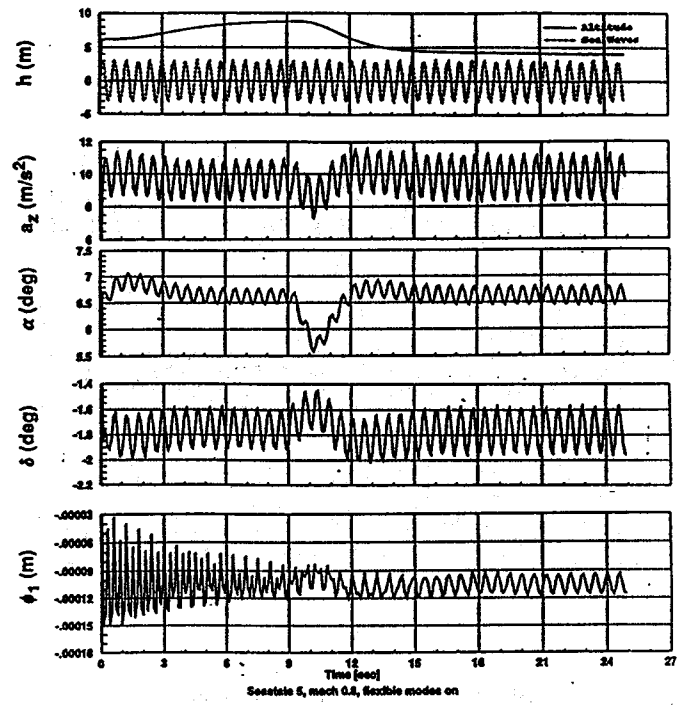

Figure 11.- Flexible simulation results for $M_\infty = 0.8$ and sea state 5.

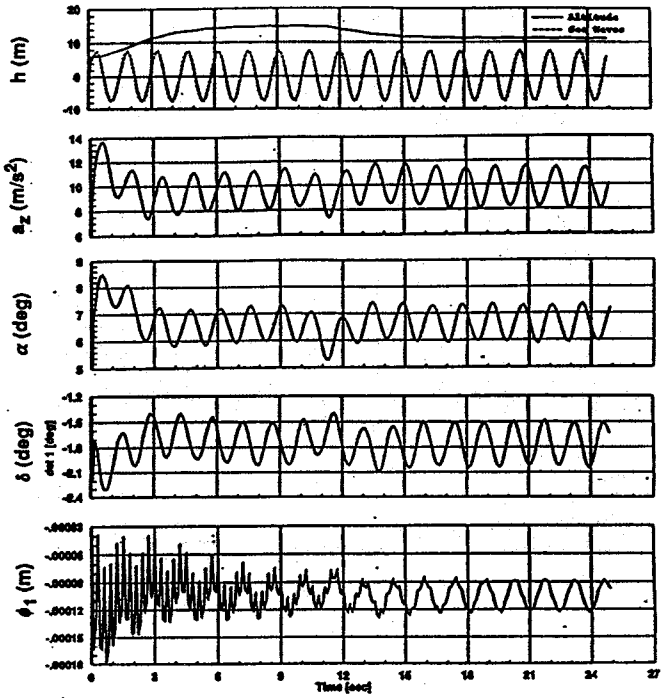

Figure 12.- Flexible simulation results for $M_\infty = 0.8$ and sea state 7.

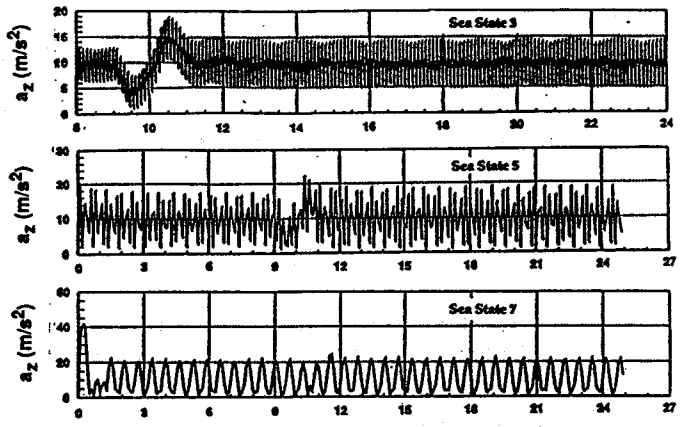

Figure 14.- Vertical acceleration for $M_\infty = 2.0$ and sea states 3, 5, and 7.

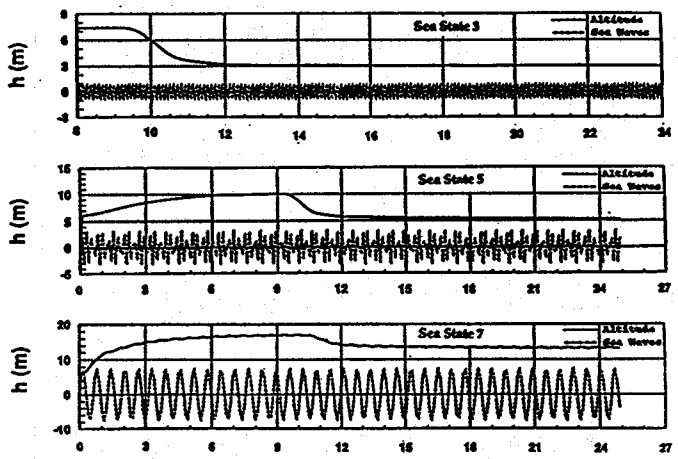

Figure 13.- Missile altitude for $M_\infty = 2.0$ and sea states 3, 5, and 7.

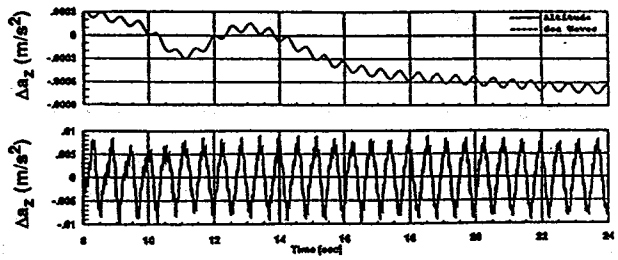

Figure 15.- Difference between flexible and rigid missile simulation results.